Supermassive Black Hole Winds in X–rays

M. Brusa[1,2], G. Matzeu[1,2], S. Bianchi[3], E. Piconcelli[4], M. Dadina[2], G. Lanzuisi[2], A. Bongiorno[4], M. Cappi[2], A. Comastri[2], D. Costanzo[1,2], G. Cresci[5], F. Duras[3], C. Feruglio[6], R. Gilli[1,2], F. La Franca[3], A. Luminari[7,4], G. Matt[3], R. Middei[8,4], E. Nardini[5], G. Ponti[9,10], F. Tombesi[11], E. Torresi[2], C. Vignali[1,2], A. Zaino[3], and L. Zappacosta[4]

[1] Dipartimento di Fisica e Astronomia "Augusto Righi", Università di Bologna, via Gobetti 93/2, 40129 Bologna, Italy
[2] Istituto Nazionale di Astrofisica - Osservatorio di Astrofisica e Scienza dello Spazio di Bologna, via Gobetti 93/3, 40129 Bologna, Italy
[3] Dipartimento di Matematica e Fisica, Università degli Studi Roma Tre, via della Vasca Navale 84, 00146 Roma, Italy
[4] Istituto Nazionale di Astrofisica - Osservatorio Astronomico di Roma, via Frascati 33, 00078 Monte Porzio Catone (RM) Italy
[5] Istituto Nazionale di Astrofisica - Osservatorio Astrofisico di Arcetri, Largo Enrico Fermi 5, 50125 Firenze, Italy
The remaining affiliations can be found at the end of the paper.

Abstract. SUBWAYS (Supermassive Black Hole Winds in X-rays) is an international program designed to provide a unique observational framework to test the validity of physical models for Active Galactic Nuclei (AGN) outflows. Its ultimate goal is to understand the AGN impact onto their host galaxies. Within this framework, we have been awarded a Large Program of ~1.4 Ms with XMM-*Newton* in AO18, to observe a representative sample of 17 objects at z=0.1-0.5, above the knee of the AGN luminosity function with the main goal of obtaining a statistically sound estimate of the duty cycle and physical parameters of ultra-fast outflows (UFOs).

We present here the first results from the data reduction and analysis of the AO18 XMM-Newton datasets. By performing a statistically driven blind line-search coupled with extensive Monte Carlo simulations, we find that absorption lines corresponding to highly ionised Fe K xxv Heα and Fe K xxvi Lyα, are detected in 7/17 sources at a $P_{\mathrm{MC}} \gtrsim 90\%$ significance level and hence corresponding to ~ 40% of the sample. The results of this work are consistent with those previously obtained in the local and high-z Universe, and independently provide a further support for the existence of highly ionised matter propagating at mildly relativistic speed ($\gtrsim 0.1c$) in a considerable fraction of AGN in the intermediate Universe.

1. Introduction

It has been proposed that gas flows in the form of energetic winds may play a pivotal role in galaxy evolution (e.g. King & Pounds 2015). Their presence may regulate both accretion and ejection of material onto and from the Supermassive Black Holes (SMBH, 10^6-10^{10} M⊙) sitting in the nuclei of virtually all galaxies. In addition, the gas accelerated by the radiation pressure from the accretion disc in sources accreting near the Eddington limit interacts with the host galaxy Interstellar Medium (ISM), propagating momentum and energy and providing an efficient feedback mechanism (e.g. Zubovas & King 2012).

The ISM of galaxies includes gas in various phases, spanning from the cold and dense molecular clouds to the very hot, highly ionized medium. Analogously, the outflows developing in AGN host galaxies have a multiphase nature, as revealed by observations and expected from simulations (Cicone et al. 2018; Veilleux et al. 2020; Nelson et al. 2019). Theoretical models ascribe an important role to relativistic hot outflows produced by the innermost gas close to the accretion disk (< 1 pc) that first feels the AGN radiation field (King 2005). Within this region, AGN-driven winds are detected routinely as absorption lines in the Ultraviolet (e.g. BAL QSOs, Crenshaw et al. 2003), and in soft X-ray spectra (0.3-1 keV, warm-absorbers, WAs) of a substantial fraction of AGN (> 50%, e.g. Reynolds 1997; Piconcelli et al. 2005). These features reveal photo-ionized material flowing outward from the nucleus with typical velocities of 10^2-10^3 km s^{-1}. Winds with extreme velocities (Ultra-Fast Outflows, UFOs, v≳0.1c) are also detected at higher energies, through strongly blue-shifted absorption lines associated with highly ionized iron ions (Fe xxv and Fe xxvi) observable at E>7 keV (Chartas et al. 2002; Pounds & Reeves 2009)), with mass outflow rates typically of 0.1-1 M⊙/yr (Tombesi et al. 2010). A detailed modeling of the high energy spectra of the most powerful QSO hosting X-ray winds, PDS456, indicates that they are weakly collimated, wide angle outflows involving a significant kinetic power of 2-3×10^{46}

erg s^{-1} , e.g. ∼20-30% of the bolometric luminosity depending on the covering factors measured (Nardini et al. 2015; Luminari et al. 2018, assuming respectively 2π and 2.8π for the opening angle).

Outflows are also routinely observed at host galaxy scales, in the ionised, neutral/atomic and molecular gas phases, with sensitive optical/FIR/mm/radio facilities (e.g. Morganti et al. 2005; Feruglio et al. 2010; Harrison et al. 2014; Cresci et al. 2015). These fast moving gas components observed at kpc scale or beyond show lower velocities with respect to the accretion disc winds (v∼ 500 − 2000 km s^{-1}, depending on the phase), and mass outflow rates up to 100-1000 M⊙/yr (see Cicone et al. 2018). The investigation of the driving mechanism of the accretion disc winds, the connection with the winds observed up to kpc scales, and the study of how the activity of the BH in the very center of a galaxy influences its properties up to its boundaries are nowadays some of the hottest topics in extragalactic astrophysics, and are part of the core science programs of future astronomical facilities, from millimeter wavelengths (Combes 2013) to optical/infrared (e.g. Padovani et al. 2017) to X-rays (Barret & Cappi 2019).

From an observational point of view, the characterisation of the fastest component of accretion disc winds in terms of physical properties (e.g. velocities, mass outflow rates, duty cycle), and their incidence in relation to the AGN properties, has been mainly carried out so far through inhomogeneous studies of archival data. The studies have been focusing on two cosmic epochs merely for practical reasons: 1) at z<0.1, objects are close enough that it is relatively easy to collect > 10000 counts in the 4-10 keV band in large samples (> 50 objects), but mainly limited to Seyfert luminosities (L_{bol}≲10^{45} erg s^{-1}, e.g. Tombesi et al. 2010; Gofford et al. 2013); 2) at z≳1.5, on small and sparse samples (<10 objects) at L_{bol}≳10^{46} erg s^{-1} (e.g. Chartas et al. 2009; Dadina et al. 2016; Vignali et al. 2015). The distribution of these two samples in the luminosity-redshift plane is shown in the upper panel of Fig. 1 (blue and magenta points, respectively). In order to gain significant advances in our understanding
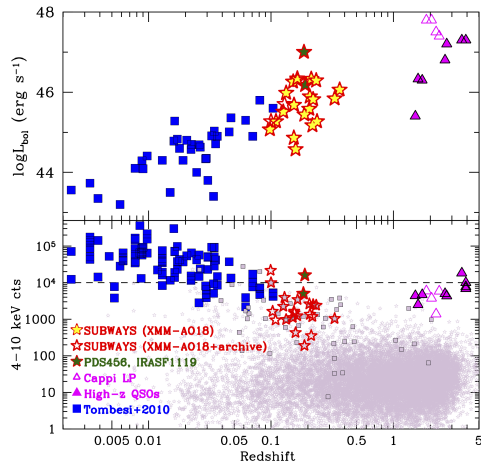
Fig. 1. The luminosity (upper panel) and rest frame 4-10 keV counts (lower panel) plotted against redshift for the samples considered in the selection process and in the comparison samples, as labelled.

of the detection rate and physical properties of UFOs, a systematic approach is needed to increase the number of sources well-exposed in X–rays in the QSO-like regime at z> 0.1.

2. Sample selection and observations

The SUBWAYS ("Supermassive Black Hole Winds in X-rays) program is designed to provide a direct test of QSO feedback models via observations of $\sim$ 20 sources at z=0.1-0.5 and $L_{bol} > 10^{45}$ erg/s, carefully selected to overcome the limitations described above. We selected the targets for the dedicated XMM-*Newton* observations according to the following requirements:

1. presence in the 3XMM-DR7 catalog[1], matched to the SDSS-DR14 catalog[2], or to the Palomar-Green Bright QSO catalog (PG QSO; Schmidt & Green 1983). This step assures that an assessment of the count-rate already exists, and it was crucial to tune the requested observing time;

---

[1] http://xmmssc.irap.omp.eu/Catalogue/3XMM-DR7/3XMM_DR7.html

[2] http://www.sdss.org/dr14/

2. redshift in the range z=0.1-0.5. This step ensures that both WAs and UFOs can be studied and at the same time, provides the possibility to characterise the continuum up to 10 keV;

3. count rate larger than $\sim$0.12 cts/s in the rest-frame 4-10 keV band, to ensure that our targets are QSOs ($L_{bol} \gtrsim 10^{45}$ erg s^{-1}; stars in the upper panel of Fig. 1), complementing what already available in the archive for this kind of studies. This step should also ensure that $\sim$5000-10000 counts needed to fulfil our goals are obtainable within a single XMM-*Newton* orbit. We recall that the analysis of PDS456 and IRASF11119 (two of the best examples of UFOs) has been conducted with a similar counting statistics (Nardini et al. 2015; Tombesi et al. 2015).

4. We further discarded NLSys (because of the highly variable flux), and quasars in clusters/radio loud systems, to avoid contamination by processes other than AGN accretion and winds.

Twenty four objects satisfied our selection criteria, tuned to populate the so-far under-explored luminosity range $L_{bol} \simeq 10^{45-46}$ erg s^{-1} with unprecedented quality X-ray spectra. The lower panel of Fig.1 shows the available rest-frame 4-10 keV counts for the SUBWAYS sample at the end of 2018 (large stars), compared to those in 3XMM-SDSS, 3XMM-PGQSO and local and high-z UFOs samples (see labels and caption for details).

Five sources (PG1114+445, PG1416-129, PG1402+261, PG0804+761 and HB89 1257+286) have already $\gtrsim$10000 counts in archival observations (see e.g. Serafinelli et al. 2019; Porquet et al. 2007; Reeves et al. 2004). We have been awarded XMM-Newton observations for 17 of the remaining 19 sources (red stars). In this paper we highlight a quick description of the data analysis procedure, the first results on the UFOs detection fraction in the observations of our XMM-*Newton* large program, and the future perspectives for the SUBWAYS project. The presentation of the results for the full SUBWAYS sample, including a detailed

Table 1. [1] Source name; [2] Redshift; [3] Starting date of observation; [4] Net exposure after background optimization; [5]pn total net counts in the 4−10 keV band.

Source[1]	ObsID	redshift[2]	Date[3]	Net Exposure[4]	Total counts[5]
		z	yyyy-mm-dd	ksec (pn)	counts (pn)
PG0052+251	0841480101	0.154	2019-07-15	34.4	9119
PG0953+414	0841480201	0.234	2020-04-14	45.5	5244
PG1626+554	0841480401	0.133	2019-05-27	51.4	5902
PG1202+281	0841480501	0.164	2020-06-29	46.8	7141
PG1435−067	0841480601	0.126	2019-07-24	42.3	2022
SDSS J144414+0633	0841480701	0.207	2019-07-28	66.3	7067
2MASS J165315+2349	0841480801	0.103	2020-02-11	59.8	7652
PG1216+069	0841480901	0.331	2020-06-05	63.4	4792
PG0947+396	0841481001 (Obs 1)	0.205	2019-11-25	31.1	1682
	0841482301 (Obs 2)		2020-04-17	45.7	2436
WISE J053756−0245	0841481101	0.110	2020-03-02	69.8	3900
HB 891529+050	0841481301	0.218	2019-08-22	75.3	3592
PG1307+085	0841481401	0.154	2020-01-22	73.1	10547
PG1425+267	0841481501	0.364	2020-02-05	73.3	4708
PG1352+183	0841481601	0.151	2020-01-26	74.4	3951
2MASS J105144+3539	0841481701	0.159	2020-05-26	80.3	2139
2MASS J0220−0728	0841481901	0.213	2020-02-03	77.1	3856
LBQS 1338−0038	0841482101	0.237	2020-02-01	91.6	7775

Table header spanning: *Optimised EPIC Data Reduction:4−10 keV Band*

comparison with literature samples at low and high-z, will be presented in a forthcoming paper (Matzeu et al. 2022)
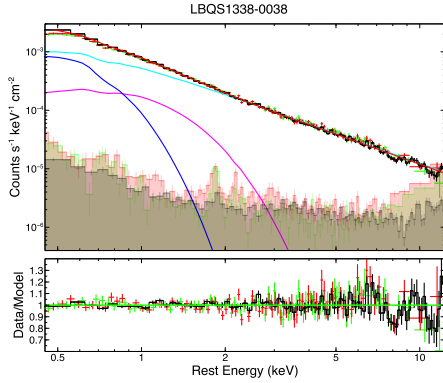

Fig. 2. The 0.3–10 keV (rest-frame) data and best-fit continuum of the Type 1 QSO LBQS1338. Top: background subtracted XMM-*Newton* spectra: EPIC-pn (black), EPIC-MOS 1 (red), EPIC-MOS 2 (green) and their corresponding background levels (shaded areas). Broadband best-fit continuum model (solid red) is plotted over the data, together with the individual model components: absorbed power-law (cyan), blackbody-low (blue) -high (magenta). Bottom: Corresponding residuals of the data compared to the best-fitting model.

2.1. XMM-Newton AO18 observations

The XMM-*Newton* observations took place over a time frame of more than one year, from May 27th 2019 to June 29th 2020. The targets have been exposed between 40 and 110 ks, depending on the count rate. Table 1 reports the list of targets, the redshifts and the log of observations.

We analysed both the EPIC-pn and MOS1,2 data and we used the procedure described in Bianchi et al. (2009) and Piconcelli et al. (2004) to filter the data from high background flares and to evaluate the best source extraction radius (see Matzeu et al. 2022 for more details). The last two columns of Table 1 list the pn exposure time after background flare filtering and the pn counts in the 4-10 keV energy band. The total counts including the MOS1 and MOS2 data are a factor of ∼ 2 larger than those in the pn only.

We then extracted the spectra using standard pipeline procedures and we generated the response files with the SAS tasks RMFGEN and ARFGEN with the latest calibration files. For the spectral binning, we chose to adopt the Kaastra & Bleeker (2016, KB hereafter) optimal binning, after extensively testing four of the most widely used spectral binning options in literature (all discussed in Matzeu et al. 2022). For reference, for all the 17 targets, the KB bin-

ning produced a EPIC-pn bin widths ranging between $\Delta E \sim 120 - 150$ eV at 6.4 keV.

3. Spectral analysis

The spectral analysis has been performed using XSPEC (version XX.XX). All the spectra were fitted with a simple power-law (`zpow` in XSPEC) and their corresponding Galactic absorption (modelled with `Tbabs` in XSPEC) , with column densities obtained from the HI4PI Collaboration et al. (2016) survey. In order to better constrain the properties of the underlying continuum, we considered additional model components to account for the spectral complexity, such as the presence of intrinsic warm or neutral absorption components (modelled with `Xabs` in XSPEC) or the presence of the soft excess (modelled with one or two `zbbody` components in XSPEC).

An example of the adopted continuum modeling applied to one of our targets (LBQS 1338−0038) is shown in Fig. 2. The background subtracted XMM-*Newton* spectra of EPIC-pn (black), EPIC-MOS 1 (red), and EPIC-MOS 2 (green) are shown with their corresponding background levels (shaded areas). The broadband best-fit continuum model is marked by the solid red line, together with the individual model components: absorbed power-law (cyan), and the two blackbody components at low (blue) and high (magenta) temperatures. Residuals at energies in the 6-10 keV range are clearly present (bottom panel in Fig. 2).

3.1. Search for absorption (and emission) features

Once an acceptable fit of the 0.3–10 keV spectra of each of the 17 sources had been reached, we performed a systematic search for iron K emission and absorption profiles through blind-line search via energy–intensity plane contours plots, as introduced in Miniutti et al. (2009). The blind search is performed adopting as baseline model the best fit power-law in the 0.3–10 keV band and an additional unresolved Gaussian line. The energy of the Gaussian is scanned across the spectra in the rest-frame 5–

10 keV energy range, with intervals of 25–50 eV, whereas the normalization is allowed to probe the intensity of the spectral lines both in a positive and negative direction in 250 steps. Modeling the Fe K features with Gaussian profiles allows us to characterize the significance and intrinsic properties (i.e. centroid energy, shape, width, overall strength with respect to the continuum) of the lines across the sample.

By running the search, each individual step in the energy-intensity plane is recorded into a file together with the corresponding variation of the Cash[3] statistics ($|\Delta C_{line}|$) from the best-fit of the continuum so that its distribution can be revealed with respect to the baseline model. The resulting confidence contours are plotted according to a mapped ΔC deviation of -2.3, -4.61, -9.21, -13.82 and -18.52 for 2 parameters of interest corresponding to 68%(1σ), 90%, 99%, 99.9 and 99.99% confidence levels.

Figure 3 shows an example of the application of the blind search method to the EPIC-pn spectrum of the source shown in Fig. 2. In the top panel we show the unfolded EPIC-pn spectrum fitted only with the best fit continuum model. The vertical dashed lines denote the position of the laboratory energy transition of Fe Kα (6.400 keV) and Fe xxv (6.70 keV) transitions, from left to right. On the bottom panel we show the resulting energy–intensity contours map, showing the presence of a highly significant emission and absorption component (see colour map on the right) at centroid rest-frame energies of $E_{em} \sim 6.6$ keV and $E_{abs} \sim 8$ keV, respectively. Both the emission and absorption lines have comparable width and the emission (as well as the absorption) seems to be originating from ionized material. Such features remind us of the P-Cygni like profile detected in PDS456 (Nardini et al. 2015) where the emission component arises from photons scattered back to our line of sight from the same outflowing ionized gas averaged from all viewing angles.

---

[3] The KB binning uses a binning scheme based on the resolution of the detector and the available photons. This implies that Cash statistics is better suited than the chi square statistics, based on a fixed number of counts per bin.
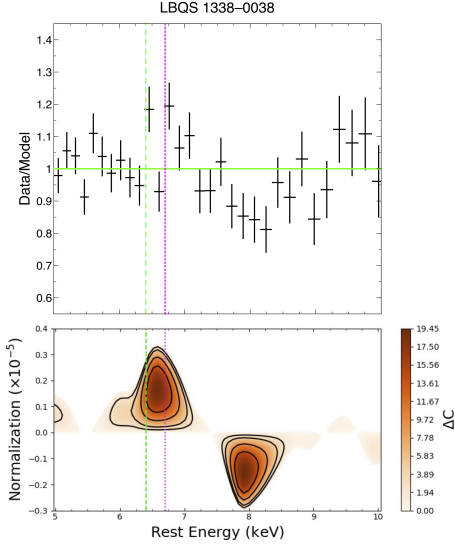
Fig. 3. Bottom panel: the results of the blind-search approach applied to LBQS 1338−0038. A strong emission line at high confidence level is detected with centroid energy of $E_{em} \sim 6.6$ keV. A Fe absorption feature is also significantly detected at $E_{abs} \sim 8$ keV. The significance contours corresponds to 68%, 90%, 99% and 99.9% from outer to inner. Top panel: the unfolded EPIC-pn spectrum data/model ratio, when fitted with the best fit continuum only (see text in Sect. 3).

3.2. Incidence of blueshifted absorption features

Overall, among these 17 targets we detected blueshifted Fe K absorption lines in 8 sources with a F-test probability, P_F, larger than 95%. As already pointed out in the literature (e.g., Porquet et al. 2004; Markowitz et al. 2006; Tombesi et al. 2010; Parker et al. 2020), the F-test and goodness of fit likely over-predict the detection probability as opposed to an extensive Monte Carlo (MC) simulation approach.

We therefore performed MC simulations in order to quantify the detection significance against random fluctuations and noise in the spectrum on all the 8 Fe K absorption line candidates detected at $P_F \gtrsim 95\%$ confidence level. We simulated S=1000 EPIC-pn spectra by us-

ing the `fakeit` command in XSPEC and assuming for each source its best-fit 0.3–10 keV broadband continuum model. The simulated spectra were generated with the same exposure times and response files from the original data. A narrow Gaussian of 10 eV was then added to the fitting model, initially at $E_{rest} = 6$ keV with normalization set to zero and free to vary between negative and positive values in order to probe both absorption and emission features. The rest energy centroid of the Gaussian line was stepped between the rest frame energies of $E = 5.5$–9.5 keV in $\Delta E = 25$ eV increments with the STEPPAR command in XSPEC. This process maps the ΔC variations relative to C_{null} and are recorded after each step as $|\Delta C_{noise}|$.

The initial significance of the line derived from the real data $|\Delta C_{line}|$ was compared to the $|\Delta C_{noise}|$ distribution so that the number N of simulated spectra with a random noise fluctuation $|\Delta C_{noise}| \geq |\Delta C_{line}|$ can be evaluated and the MC statistical significance of the absorption line detection can be calculated as $P_{MC} = 1 - \left(\frac{N}{S}\right)$. Of the 8 blueshifted Fe K absorption detections with $P_F > 95\%$, 5 have $P_{MC} > 95\%$.

3.3. Detection fraction and typical velocities

We revealed the presence of significant blueshifted Fe K absorption tracing UFOs in 5 out of 17 targets, corresponding to $\sim$ 30% of the sample. The velocity distribution ranges from 0.075c to 0.3c, with a mean value at v$\sim$0.165c.

Based on a similar analysis, counting statistics and assessment of detection significance, Tombesi et al. (2010) reported a UFO detection fraction of 30-40% in a sample of 42 local AGN (z< 0.1), with a mean velocity of v$\sim$0.1c. The detection fraction and the observed velocities in the SUBWAYS sources observed in the XMM-*Newton* AO18 program are therefore consistent with the values measured in local samples. This is the first time the incidence of UFOs has been determined in a statistical significant sample of quasars beyond the local Universe.

4. Perspectives

The first results presented in this work will be strengthened by extending the analysis of the AO18 sample to the full SUBWAYS sample, including the archival data (Matzeu et al. 2022), and combining results from this program with X–ray data of local Seyferts (Tombesi et al. 2010; Gofford et al. 2013) and high-redshift QSOs (e.g. the compilation reported in Chartas et al. 2021, see also Dadina et al. this issue). More in details:

- it will be possible to explore in its entirety the luminosity-redshift plane to look for correlations of the winds and nuclear properties over a wide range in AGN power (3-4 dex). We will therefore investigate how the detection rate of UFOs changes as a function of AGN radiative luminosity, black hole mass Eddington ratios.
- Estimating the energetics of the nuclear winds and comparing it with that of larger-scale ionised and molecular outflows provides crucial constraints on the wind propagation mechanism and on the amount of energy that is transferred to the kpc scale (e.g. Tombesi et al. 2015). Such a comparison has so far been attempted only in few sources, via deep observations at X-ray and millimeter wavelengths, with contradicting results, that challenge the energy conserving scenario for the outflow propagation, at least for the most luminous sources (e.g. Nardini & Zubovas 2018; Sirressi et al. 2019; Marasco et al. 2020). With this enlarged sample we will be able to test models which drive outflows purely via radiative power (e.g., King 2010) or with a combination of other mechanisms not necessarily linked to Eddington ratios (e.g., Sądowski & Gaspari 2017).
- In addition, it is important to take into account special relativity effects in order to correctly assess the mass and energy outflow rates of UFO. In fact, owing to space-time transformation, the opacity of the gas drops for increasing velocity v_{out}; as a result, the observed (i.e. apparent) column density measured through spectral fitting has to be corrected according to v_{out} to derive the intrinsic gas column N_H (Luminari et al. 2020; Laurenti et al. 2021). This correction amounts to a factor 20-120% for $v_{out} = 0.1 - 0.3c$, and linearly propagates to the mass and energy outflow rates. Given the very high velocities observed in our SUBWAYS sample, neglecting such effects would result in a significant underestimate of the wind energies and, then, of the feedback potential on the host galaxies.
- The XMM-*Newton* observations are only a first step for a comprehensive multi-wavelength approach in the topic of multiphase outflows investigation and their connection with host galaxy properties. We already secured follow-up campaigns in the hard X–rays with NuSTAR (PI: S. Bianchi, ∼ 500 ks), in the UV with HST (PI: J. Kriss, ∼ 25 orbits), at millimeter with NOEMA (PI: C. Feruglio, 9 targets) and in the radio band with LOFAR (PI: R. Morganti, all targets) and VLA (PI: F. Panessa, 20.35 hours). SUBWAYS is setting the stage for the first, truly physically motivated investigation of multi-phase gas in AGN in quasars host galaxies.

Affiliations

[6] Istituto Nazionale di Astrofisica Osservatorio Astronomico di Trieste, Via Tiepolo 11, I-34131 Trieste, Italy

[7] Istituto Nazionale di Astrofisica - Istituto di Astrofisica e Planetologia Spaziali di Roma, Via del Fosso del Cavaliere, 100, 00133 Roma RM

[8] ASI-Unità di Ricerca Scientifica, Via del Politecnico snc, 00133 Roma, Italy

[9] Istituto Nazionale di Astrofisica - Osservatorio Astronomico di Brera, Via E. Bianchi 46, 23807 Merate (LC), Italy

[10] Max-Planck-Institut für Extraterrestrische Physik, Giessenbachstrasse, 85748 Garching, Germany

[11] Dipartimento di Fisica, Università di Roma Tor Vergata, Via della Ricerca Scientifica 1, I-00133 Roma, Italy

References

Barret, D. & Cappi, M. 2019, A&A, 628, A5

Bianchi, S., Guainazzi, M., Matt, G., Fonseca Bonilla, N., & Ponti, G. 2009, A&A, 495, 421

Chartas, G., Brandt, W. N., Gallagher, S. C., & Garmire, G. P. 2002, ApJ, 579, 169

Chartas, G., Cappi, M., Vignali, C., et al. 2021, ApJ, 920, 24

Chartas, G., Kochanek, C. S., Dai, X., Poindexter, S., & Garmire, G. 2009, ApJ, 693, 174

Cicone, C., Brusa, M., Ramos Almeida, C., et al. 2018, Nature Astronomy, 2, 176

Combes, F. 2013, in 11th Hellenic Astronomical Conference, 3–3

Crenshaw, D. M., Kraemer, S. B., & George, I. M. 2003, ARA&A, 41, 117

Cresci, G., Mainieri, V., Brusa, M., et al. 2015, ApJ, 799, 82

Dadina, M., Vignali, C., Cappi, M., et al. 2016, A&A, 592, A104

Feruglio, C., Maiolino, R., Piconcelli, E., et al. 2010, A&A, 518, L155

Gofford, J., Reeves, J. N., Tombesi, F., et al. 2013, MNRAS, 430, 60

Harrison, C. M., Alexander, D. M., Mullaney, J. R., & Swinbank, A. M. 2014, MNRAS, 441, 3306

HI4PI Collaboration, Ben Bekhti, N., Flöer, L., et al. 2016, A&A, 594, A116

Kaastra, J. S. & Bleeker, J. A. M. 2016, A&A, 587, A151

King, A. 2005, ApJ, 635, L121

King, A. & Pounds, K. 2015, ARA&A, 53, 115

King, A. R. 2010, MNRAS, 402, 1516

Laurenti, M., Luminari, A., Tombesi, F., et al. 2021, A&A, 645, A118

Luminari, A., Piconcelli, E., Tombesi, F., et al. 2018, A&A, 619, A149

Luminari, A., Tombesi, F., Piconcelli, E., et al. 2020, A&A, 633, A55

Marasco, A., Cresci, G., Nardini, E., et al. 2020, A&A, 644, A15

Markowitz, A., Reeves, J. N., & Braito, V. 2006, ApJ, 646, 783

Miniutti, G., Ponti, G., Greene, J. E., et al. 2009, MNRAS, 394, 443

Morganti, R., Tadhunter, C. N., & Oosterloo, T. A. 2005, A&A, 444, L9

Nardini, E., Reeves, J. N., Gofford, J., et al. 2015, Science, 347, 860

Nardini, E. & Zubovas, K. 2018, MNRAS, 478, 2274

Nelson, D., Pillepich, A., Springel, V., et al. 2019, MNRAS, 490, 3234

Padovani, P., Combes, F., Diaz Trigo, M., et al. 2017, arXiv e-prints, arXiv:1705.06064

Parker, M. L., Alston, W. N., Igo, Z., & Fabian, A. C. 2020, MNRAS, 492, 1363

Piconcelli, E., Jimenez-Bailón, E., Guainazzi, M., et al. 2004, MNRAS, 351, 161

Piconcelli, E., Jimenez-Bailón, E., Guainazzi, M., et al. 2005, A&A, 432, 15

Porquet, D., Reeves, J. N., Markowitz, A., et al. 2007, A&A, 466, 23

Porquet, D., Reeves, J. N., Uttley, P., & Turner, T. J. 2004, A&A, 427, 101

Pounds, K. A. & Reeves, J. N. 2009, MNRAS, 397, 249

Reeves, J. N., Nandra, K., George, I. M., et al. 2004, ApJ, 602, 648

Reynolds, C. S. 1997, MNRAS, 286, 513

Sądowski, A. & Gaspari, M. 2017, MNRAS, 468, 1398

Schmidt, M. & Green, R. F. 1983, ApJ, 269, 352

Serafinelli, R., Tombesi, F., Vagnetti, F., et al. 2019, A&A, 627, A121

Sirressi, M., Cicone, C., Severgnini, P., et al. 2019, MNRAS, 489, 1927

Tombesi, F., Cappi, M., Reeves, J. N., et al. 2010, A&A, 521, A57

Tombesi, F., Meléndez, M., Veilleux, S., et al. 2015, Nature, 519, 436

Veilleux, S., Maiolino, R., Bolatto, A. D., & Aalto, S. 2020, A&A Rev., 28, 2

Vignali, C., Iwasawa, K., Comastri, A., et al. 2015, A&A, 583, A141

Zubovas, K. & King, A. 2012, ApJ, 745, L34